Catalysis Today 152 (2010) 104–109

Contents lists available at ScienceDirect

Catalysis Today

journal homepage: www.elsevier.com/locate/cattod

Zinc–aluminum hydrotalcites as precursors of basic catalysts: Preparation, characterization and study of the activation of methanol

Tania Montanari [a], Michele Sisani [b], Morena Nocchetti [b], Riccardo Vivani [b], M. Concepcion Herrera Delgado [b,1], Gianguido Ramis [b], Guido Busca [a,*], Umberto Costantino [b]

[a] Dipartimento di Ingegneria Chimica e di Processo, Università di Genova, P.le J.F. Kennedy, I-16129 Genova, Italy
[b] CEMIN, Centro di Eccellenza sui Materiali Innovativi Nanostrutturati, Dipartimento di Chimica, Università di Perugia, Via Elce di Sotto, 8 - I-06123 Perugia, Italy

ARTICLE INFO

Article history:
Available online 30 October 2009

Keywords:
Zinc aluminate
Zinc–aluminum hydrotalcite
Hydrotalcite-like structure
Methanol adsorption
Transesterfication
Polyethoxylation
IR spectroscopy
Acid–base catalyst

ABSTRACT

Monophasic ZnAl hydrotalcite-like layered hydroxycarbonate has been prepared by the urea precipitation method. This material has been characterized by Rietveld refinement of the XRPD pattern, DTA-TG and skeletal IR. ZnAl mixed oxides have been prepared by calcinations of this precursor. According to XRPD, after calcinations at 450 °C this material is constituted by poorly crystallized ZnO phase. IR spectroscopy shows the presence of additional spinel-like domains. The surface of this catalyst is dominated by poorly acidic Zn^{2+} cations and terminal and bridging hydroxy groups bonded to Zn ions. This catalyst adsorbs methanol dissociatively giving rise to two types of methoxy groups. Type A, likely bridging on Al and Zn ions, is more stable to desorption. Type B, likely terminally bonded to Zn^{2+} cations, is more labile with respect to decomposition into CO and H_2. Type B methoxy groups appear to be very ionic and are, likely, those involved in transesterification and polyethoxylation reactions. ZnO and $ZnAl_2O_4$ particles progressively crystallize and sinter by increasing calcination temperature.

1. Introduction

Zinc aluminates, either stoichiometric or containing an excess of zinc, were characterized in earlier studies as very basic materials [1,2]. In fact, ZnAl mixed oxides find practical application as catalysts for industrial processes which have been classified as typically base-catalyzed, although an acid–base cooperation certainly occurs with solid catalysts [3,4]. They are reported to act as the industrial catalysts of the Institut Français du Pétrol (IFP) process for the biodiesel synthesis by transesterification of fats (Esterfip-H process [5]) as well as of polyethoxylation processes producing non-ionic surfactants (Henckel, BASF [6,7]). Zinc aluminate has also been patented as an optimal catalyst for light olefins double bond position isomerization (Phillips [8]).

Zn aluminates are also supports or components of relevant industrial catalysts such as, in particular, copper containing catalysts for methanol synthesis [9,10], low temperature water gas shift [9,10] and for hydrogen production from methanol steam reforming [10–12]. They are also components of promising Ni catalysts for hydrogen production by ethanol steam reforming [13]. These catalysis behaviors are thought to be assisted by basicity [3].

Like Mg aluminates, Zn aluminates may be prepared by thermal decomposition of hydrotalcite-type precursors. Hydrotalcites (HTs), i.e. Mg–Al layered double hydroxides, and the products of their calcination are very useful and popular basic materials which find industrial application as basic catalysts [14–17]. ZnAl hydrotalcites have been patented as precursors of catalysts for polyethoxylation of alcohols [6,7]. In spite of the relevant industrial interest for these materials, the scientific literature concerning ZnAl HT as catalysts or catalyst precursors is poor.

Both polyethoxylation and transesterification imply the activation of an alcohol as a nucleophilic reactant, to attack the electrophilic carbon of carboxylate esters (transesterification) and of ethylene oxide (polyethoxylation).

In the present communication we will refer about the preparation of ZnAl HT using the urea method, developed in one of our laboratories a few years ago [18]. Additionally, we will refer about characterization of the products of its calcinations as well as on the adsorption and activation of methanol (as a typical alcohol reactant) on them.

* Corresponding author. Tel.: +39 0103536024; fax: +39 0103536028.
E-mail address: Guido.Busca@unige.it (G. Busca).
[1] On leave from Departamento of Ingenieria Quimica, Universidad de Malaga, Malaga, Spain.

0920-5861/$ – see front matter © 2009 Elsevier B.V. All rights reserved.
doi:10.1016/j.cattod.2009.09.012

2. Experimental

2.1. Preparation procedure

HT of formula $[Zn_{0.67}Al_{0.33}(OH)_2](CO_3)_{0.165}\cdot 0.5H_2O$ was prepared by the urea method [18]. Solid urea was dissolved in a solution of 0.165 mol/dm^3 of $Al(NO_3)_3\cdot 9H_2O$ and 0.335 mol/dm^3 of $Zn(NO_3)_2\cdot 6H_2O$ to reach a urea/metal ion molar ratio of 3.3. The clear solution was maintained at 100 °C for 36 h. The obtained precipitate was separated from the mother solution, washed with de-ionized water and with small volumes of 0.1 M sodium carbonate in order to exchange residue nitrate ions with carbonate ions. After washings with Na_2CO_3 solution, the solid was recovered, washed with de-ionized water and finally dried at room temperature over P_4O_{10}.

2.2. Characterization techniques

Metal analyses were performed by Varian 700-ES series Inductively Coupled Plasma-Optical Emission Spectrometers (ICP-OES) using solutions prepared by dissolving the samples in concentrated HNO_3 and properly diluted.

Coupled thermogravimetric (TG) and differential thermal (DTA) analyses were performed with a Netzsch STA 449C apparatus, in airflow and heating rate of 10 °C/min.

The morphology of powder was examined with a Philips XL30 Scanning Electron Microscope (SEM) after having deposited a drop of the suspension of the HT in acetone on a holder and having left the solvent to evaporate at room temperature. The samples ware metallized with gold.

X-ray powder diffraction (XRPD) patterns were collected in theta–theta reflection geometry with the Cu Kα radiation on a PANalytical X'PERT PRO diffractometer, PW3050 goniometer equipped with an X'Celerator detector. The Long Fine Focus (LFF) tube operated at 40 KV, 40 mA. Data were collected using a step size of 0.017° and a count time of 40 s per step.

The IR spectra were recorded with a Nicolet Nexus Fourier Transform instrument. A conventional manipulation/outgassing ramp connected to the IR cell was used. For the analysis of the skeletal vibrations KBr pressed disks were used. For adsorption experiments pressed disks of pure catalyst powders (15 mg, 2 cm diameter) were used. The samples were thermally pre-treated in the IR cell by heating in air at 450 °C for 2 h and later by outgassing 1 h at 450 °C. The adsorption procedure involves contact of the activated sample disk with CO at 130 K in the conventional IR cell cooled with liquid nitrogen. Desorption is carried out by outgassing upon warming from 130 K to room temperature. Methanol adsorption experiments were performed at r.t., followed by outgassing at r.t. and at 110 °C. Methanol decomposition experiments were performed at 30–350 °C in static conditions with methanol 5 Torr pressure.

2.3. Rietveld refinement

Rietveld refinement of the structural model taken from Ref. [18] for the product of precipitation was performed using the GSAS program [19]. Sample displacement, cell parameters and background were first refined. Then fractional coordinates and profile shape were also refined. The profile was modeled using a pseudo Voigt profile function [20]. Inspection of the diffraction profile revealed that the pattern was affected by anisotropic peak broadening. The *00l* reflections were noticeably broader than other reflections, suggesting that the coherent diffraction domains preferentially extend along the [00l] crystallographic planes, that is the direction of growth of inorganic layers. Fixing the anisotropic broadening axis along the *00l* direction, the refined anisotropy broadening coefficients X_e and Y_e assumed positive values (0.06° and 0.66°, respectively) attesting the presence of a certain amount of shape anisotropy and defects along the direction of layer packing. Isotropic thermal factors were set to a reasonable value and not refined. Soft restraints were applied to O–H and carbonate C–O bond lengths, in order to avoid refinement unstability. The metal atom occupancies were set according to stoichiometry and were not refined. At the end of the refinement the shifts on all parameters were less than their standard deviations.

3. Results and discussion

3.1. TG-DTA and SEM analyses

Fig. 1 shows the coupled TG-DTA curves of ZnAl HT. The TG curve is characterized by a continuous mass loss without well-defined plateaux between the decomposition steps. The first mass loss of 1.8% at 100 °C, corresponding to a broad endothermic peak, can be ascribed to the loss of adsorbed water and it is followed by a second more pronounced and sharp endothermic phenomenon, due to loss of hydration water from the interlayer region at 190 °C, corresponding to the 8.5% of the total mass. A second step extends up to 400 °C, and it is assigned to the overlapped mass losses due to the dehydroxylation of the layers and the decomposition of the carbonate counter-anions as carbon dioxide. In addition, the small mass loss observed around 600 °C can be ascribed to the loss of residual surface carbonate anions and/or dehydroxylation water [21,22]. Being known the Zn/Al molar ratio and that at 1000 °C the ZnO and $ZnAl_2O_4$ are formed, it was possible to assign to the sample the following composition: $[Zn_{0.67}Al_{0.33}(OH)_2](CO_3)_{0.165}\cdot 0.5H_2O$. SEM analysis (Fig. 2) clearly reveals the lamellar morphology of the sample. The layered microcrystal aggregates are evident and a rough estimation indicates that the thickness of the each layered microcrystals is of the order of few hundreds of nm, the size being of the order of few microns.

3.2. XRPD analysis of ZnAl HT

Tables 1–3 show the refinement details, structural parameters and selected bond lengths and angles for $[Zn_{0.67}Al_{0.33}(OH)_2](CO_3)_{0.165}\cdot 0.5H_2O$ while Fig. 3 shows the Rietveld plot. In spite of the difficulties reported by some authors [23] in preparing monophasic Zn-containing HT with the urea method, monophasic ZnAl HT has indeed been obtained. Major crystallographic features are in good agreement with those reported for MgAl–CO_3 HT [18]. The structure originates from the packing of inorganic layers along the *c* crystallographic axis. These layers are made of edge connected MO_6 octahedra. These octahedra are slightly distorted, since O-M-O

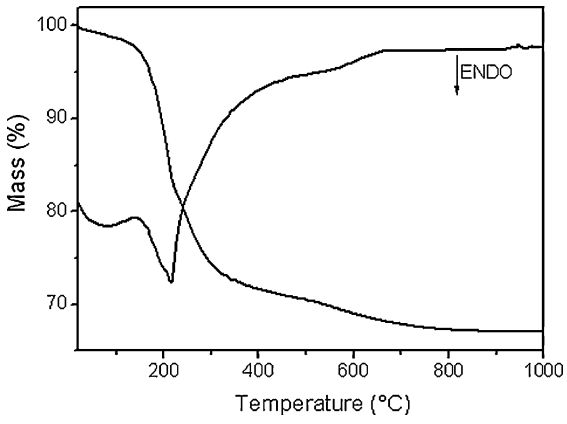

Fig. 1. TG and DTA curves of ZnAl hydrotalcite.

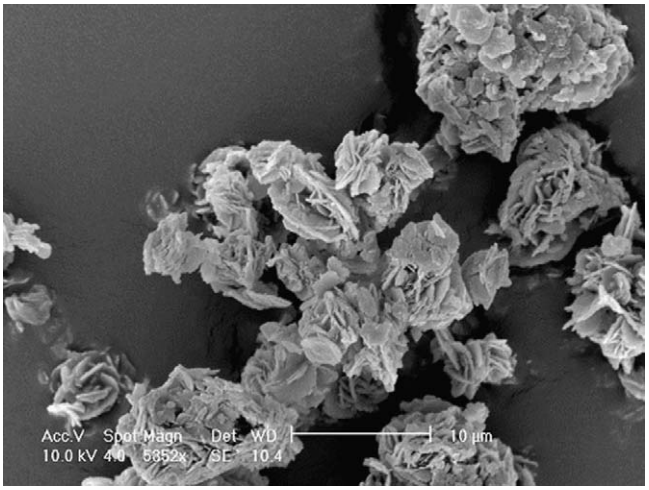

Fig. 2. SEM micrograph of ZnAl hydrotalcite.

bond angles are in the range 81.68(6)–98.32(6)°. The unit cell parameters found for ZnAl HT are larger than those reported for MgAl–CO_3 HT (a = 3.045 Å, c = 22.701 Å) [18], due to the ionic radius of Zn larger than Mg. An ordered Zn^{2+} and Al^{3+} distribution could be supposed on the bases of recent results carried out by multinuclear NMR spectroscopy on MgAl that revealed a fully ordered cations distribution for Mg:Al ratio of 2:1 [24]. The basal spacing, that corresponds to the d value of the *003* diffraction peak in the pattern, is $c/3$ = 7.59 Å. The interlayer region hosts the carbonate counter-anions and water molecules that are placed in the intermediate plane between two adjacent sheets. The molecular plane of carbonate anions is parallel to the metal planes. O(2) oxygen atoms, belonging to water or to carbonate molecules, share the same 18 h crystallographic site, just above the hydroxyl groups [O(1)], so that hydrogen bonds can form between them [O(1)···O(2) distances are 2.85(1) and 2.90(1) Å].

3.3. Skeletal IR spectrum of ZnAl HT

The skeletal IR spectrum of ZnAl HT sample (Fig. 4) is fully consistent with that presented and described in detail by Kloprogge et al. (sample 2 in [25]).

An approximate interpretation of the vibrational modes expected for this material, based on a group approximation, has been attempted. The hydrotalcite-type solids $[Zn_2Al(OH)_6](CO_3)_{0.5}\cdot 1.5H_2O$ crystallize in the $R\bar{3}m \equiv D_{3d}^5 \equiv n$ 166 space group. The full rhombohedral unit cell contains three cations, i.e. three of the above formula unit. Due to the presence of three lattice points in the overall rhombohedral unit cell, the smallest Bravais cell only contains one cation, i.e. one of the above formula unit. The Wyckoff notation does not allow to determine the cations distribution.

The structure, as already described, is formed by brucite-type layers (the same structure of brucite $Mg(OH)_2$ [26] and the isostructural hydroxides of bivalent metals such as β-$Zn(OH)_2$ [27]) with carbonate ions in the interlayer region. Obviously, there are two trivalent cations per carbonate ion. The water content is also related to the amount of trivalent cations. According to the actual composition of our solids, we have half water molecule and one sixth of carbonate ion per smallest Bravais cell.

In the OH stretching region, we expect three features in IR spectra, i.e. the antisymmetric OH stretching of the brucite-type layers and the antisymmetric and symmetric stretchings of water molecules. The position and the shape of the OH stretching modes, we observe centered at 3433 cm^{-1}, broad, is such that weak H-bonding do likely occur. The broad OH stretching band in the region 3200–2700 cm^{-1} and the H_2O scissoring mode band at 1610 cm^{-1} provide evidence of the presence of water molecules.

The lack of multiplicity of the strong band at 1359 cm^{-1}, sharp, antisymmetric stretching of the carbonate ions, provide evidence in this case of the full absence of nitrate ions, which may remain as residuals of preparation salts. The observation (weak at 1041 cm^{-1}) in the IR spectrum of the carbonate symmetric stretching mode, which is IR inactive in the highest D_{3h} symmetry, shows that its point symmetry is decreased to C_{3v}.

3.4. XRPD study of calcined ZnAl HT

As previously reported [28], the XRPD patterns taken at different temperatures show that the structure is retained up to about 140–150 °C (Fig. 5a), with a very small pattern change. Above this temperature, the XRPD pattern becomes very broadened and the structure collapses. Crystallization of ZnO starts to appear at about 350 °C, while no phases containing aluminum are initially detected. The pattern of the sample after treatment at 450 °C for 1 h (Fig. 5b) shows, although very broadened, only ZnO peaks, and no other phases can be detected. A lamellar shape with thin almost elliptical particles is observed by SEM, which recalls the original precursor particle shape, as evidence of the topotactical nature of the hydrotalcite decomposition step. The measured BET surface area of this sample is 80 m^2/g.

Table 1
Crystallographic data for $[Zn_{0.67}Al_{0.33}(OH)_2](CO_3)_{0.165}\cdot 0.5H_2O$.

Crystal system	Trigonal
Space group	$R\bar{3}m$
a/Å	3.0748(1)
c/Å	22.7685(5)
Cell volume/Å^3	186.423(6)
Z	3
Calculated density/g·cm^{-3}	2.82
Unit cell formula weight/uma	316.84
Wavelength/Å	1.54056
R_p[a]	0.067
R_{wp}[b]	0.086
R_F2[c]	0.057
GOF[d]	3.7

[a] $R_p = \sum|I_o - I_c|/\sum I_o$.
[b] $R_{wp} = [\sum w(I_o - I_c)^2/\sum wI_o^2]^{1/2}$.
[c] $R_F2 = \sum|F_o^2 - F_c^2|/\sum|F_o^2|$.
[d] $GOF = [\sum w(I_o - I_c)^2/(N_o - N_{var})]^{1/2}$.

Table 2
Fractional atomic coordinates and isotropic thermal parameters for $[Zn_{0.67}Al_{0.33}(OH)_2](CO_3)_{0.165}\cdot 0.5H_2O$.

Name	x/a	y/b	z/c	U_{iso} (Å^2)	Wyckoff notation	Occupancy	Number of atoms per unit cell
Zn	0.0	0.0	0.0	0.02	3a	2/3	2
Al	0.0	0.0	0.0	0.02	3a	1/3	1
O(1)	0.0	0.0	0.37678(8)	0.02	6c	1	6
C	1/3	2/3	0.4988(6)	0.02	6c	1/12	0.5
O(2)	0.1154(6)	−0.1154(6)	0.4988(6)	0.02	18h	1/6	3
H	0.0	0.0	0.4225(4)	0.02	6c	1	6

U_{iso} (Å^2) = isotropic thermal displacement parameter.

Table 3
Selected bond lengths and angles for $[Zn_{0.67}Al_{0.33}(OH)_2](CO_3)_{0.165}\cdot 0.5H_2O$.

Bond	Length/Å
Zn,Al–O(1)	2.032(1)
C–O(2)	1.161(3)
O(2)–H	1.04(1)
O(1)···O(2)	2.85(1)
O(1)···O(2)	2.90(1)
Bond angle	**Angle/degrees**
O(1)–Zn,Al–O(1) #1	98.32(6)
O(1)–Zn,Al–O(1) #2	81.68(6)
O(2)–C–O(2)	119.9(1)

By increasing the temperature (Fig. 5c and d), the pattern evolves in two well distinguished phases, that can be assigned to ZnO and $ZnAl_2O_4$, Inorganic Crystal Structure Database (ICSD) codes: 065120 and 075091, respectively. This can indicate that after decomposition of the hydrotalcite phase, aluminum tends to remain in a mixed oxide phase, which is amorphous at 450 °C and slowly separates as a crystalline phase at higher temperatures.

3.5. IR studies of the surface and bulk properties of calcined ZnAl HT.

The skeletal IR spectrum of ZnAl oxide calcined at 450 °C (Fig. 6b) shows well evident bands at 785, 700 and 485 cm^{-1}, together with a weak component at 220 cm^{-1} evident in the Far IR spectrum. This spectrum is definitely different with respect that of ZnO powders [29,30], clearly showing features similar to those of a spinel phase ($O_h^7 = Fd3m$ space group with $Z = 8$), such as the typical doublet at 785, 700 cm^{-1}, due to the vibrations of "isolated" MO_4 tetrahedra. On the other hand this spectrum does closely match neither that of well crystallized bulk $ZnAl_2O_4$ [31–34].

XRD and IR data show that this material is actually a largely amorphous structure with some kind of intergrowth between the wurtzite and the spinel phase. We may mention that, in this respect, the Zn–Al system differs from the Mg–Al system. In fact, while the MgO structure (periclase or rock-salt) has the same oxygen packing of $MgAl_2O_4$ spinel (cubic close packing) and easily forms solid solutions with it, the ZnO wurtzite structure has the hexagonal close packing of oxide ions and should form more complex structures when combines with $ZnAl_2O_4$ spinel.

The FT-IR spectrum of the pure powder pressed disk after activation in vacuum (Fig. 7) shows absorptions in the 3800–3500 cm^{-1} range, due to the stretching vibrations of surface free hydroxy groups. In particular, two main bands at 3692 and 3595 cm^{-1} are found, with weak components at 3778 and 3733 cm^{-1}. This spectrum may be compared with those reported for stoichiometric zinc aluminate where a strong band is observed at 3695 cm^{-1} with a small shoulder at 3735 cm^{-1} [2]. We may also compare this spectrum with those of the pure oxides: on alumina, bands are observed at 3790 (shoulder), 3773, 3720, and 3675 cm^{-1}, while on ZnO, bands are observed at 3670, 3640, and 3618 cm^{-1}. According to our previous discussion [30,35,36] where we proposed a modification of the well known "Knözinger and Ratnasami" model [37] for hydroxyl groups of alumina and metal aluminates, we assign the feature at 3778 cm^{-1} to $Al_{IV}OH$ species (i.e. terminal hydroxyl groups of tetrahedrally coordinated Al ions), that at 3733 cm^{-1} to $Al_{VI}OH$ species, the main band at 3695 cm^{-1} to the superimposition of bands of ZnOH and bridging Al_2OH groups, and the band at 3595 cm^{-1} to the superimposition of bands of bridging Zn_2OH species and triply bridging Al_3OH groups.

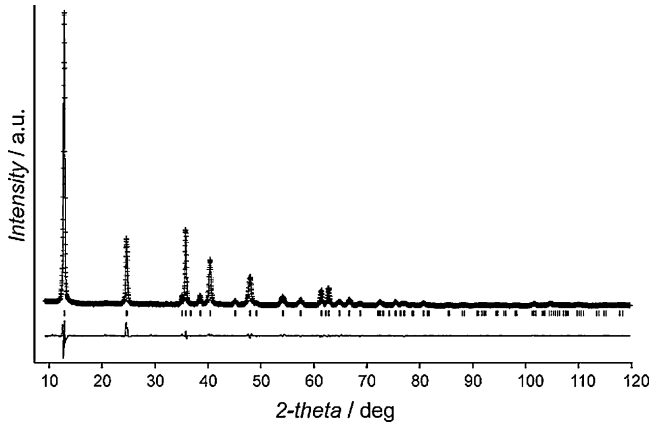

Fig. 3. XRPD pattern and Rietveld plot for ZnAl hydrotalcite. The bottom curve shows the difference between measured and calculated pattern.

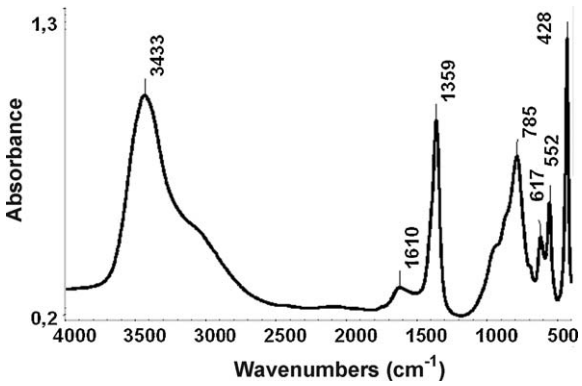

Fig. 4. Skeletal IR spectrum of ZnAl hydrotalcite (KBr pressed disk).

The strong bands 1550 and 1385 cm^{-1} with the weak feature at 1060 cm^{-1} are due to residual bulk polydentate carbonates while the sharp band at 2340 cm^{-1} is due to trapped CO_2 molecules. Both are residuals of interlayer carbonates in the interlayer region. The stability of these trapped species are evidence of the strong basicity of the bulk of this material.

The low temperature adsorption of CO over this material gives rise to a main band shifting from 2150 cm^{-1} up to 2156 cm^{-1} by decreasing coverage, and a component centered near 2185 cm^{-1}. This shows that, in spite of the formal presence of alumina, strong acid sites (i.e. Al^{3+} in incomplete tetrahedral coordination) are not

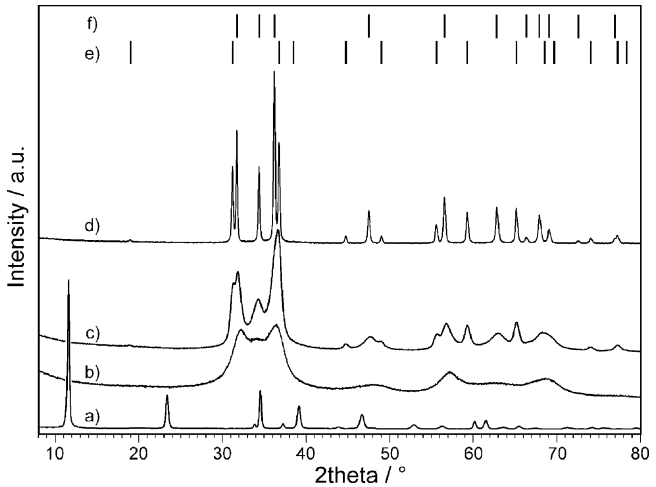

Fig. 5. XRPD patterns of ZnAl hydrotalcite taken at 140 °C (a), and at room temperature, after thermal treatment for 1 h at 450 °C (b), 750 °C (c) and 1000 °C (d). Peak positions of $ZnAl_2O_4$ (e) and ZnO (f) phases (ICSD codes: 065120 and 075091, respectively) are also reported.

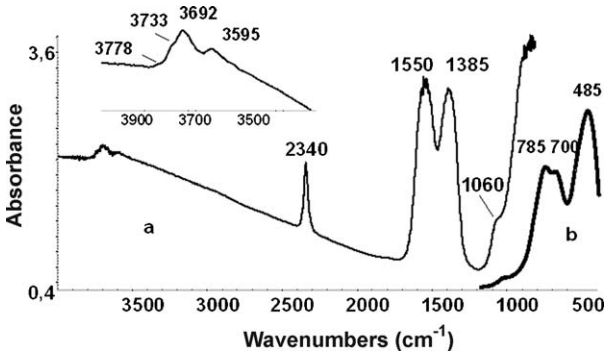

Fig. 6. IR spectra of calcined ZnAl hydrotalcite, calcined at 450 °C (a) pure powder pressed disk in situ evacuated at 450 °C; (b) skeletal spectrum, KBr pressed disk.

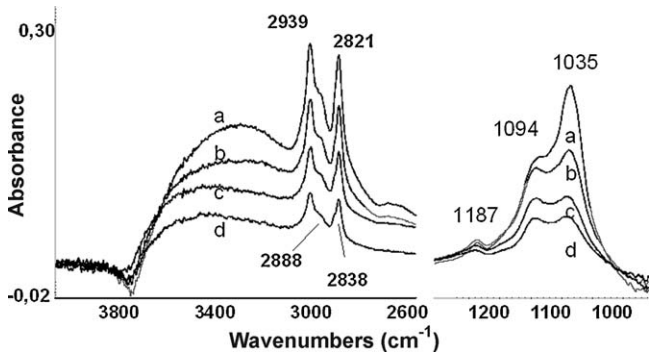

Fig. 8. IR spectra of methanol adsorbed at r.t. on calcined ZnAl hydrotalcite pure powder pressed disk activated at 450 °C in contact with the gas 30 Torr (a) and after outgassing at 30 °C (b), 60 °C (c) and 110 °C (d).

detectable. On the other hand, the spectrum of adsorbed CO is also different from that usually recorded on pure well crystallized ZnO, where bands in the 2200–2170 cm^{-1} region usually dominate, due to Zn^{2+} ions in incomplete tetrahedral coordination, corresponding to the tetrahedral coordination of Zn^{2+} in bulk ZnO. The surface of our material likely exposes Zn^{2+} ions, possibly with the copresence of Al^{3+}, but both seem to be mostly located in incomplete octahedral coordination, as in the hydrotalcite bulk. CO adsorption experiments indicate that Lewis acidity at the surface of this material is weaker than expected, based on its formal composition. The strong resistance of surface carbonate species to heating under outgassing confirms the strong basicity of this material.

3.6. IR studies of methanol adsorption on calcined ZnAl HT

In Figs. 8 and 9 the results of two experiments of methanol adsorption on the calcined ZnAl HT are reported. In Fig. 8 the spectra of the adsorbed species formed by room temperature adsorption of methanol and outgassing at increasing temperature until 110 °C are reported. The spectra in Fig. 9 are relative to contact of the catalyst with methanol 10 Torr at increasing temperature 110–400 °C. Under this experiment part of methanol decomposes to CO (well detectable in the gas phase by IR) and hydrogen, with the intermediacy of formate groups well evident in the spectra (bands at 1615, 1585 cm^{-1} and in the region 1400–1360 cm^{-1}). On the other hand, IR spectra of the gas phase also show the formation of dimethylether.

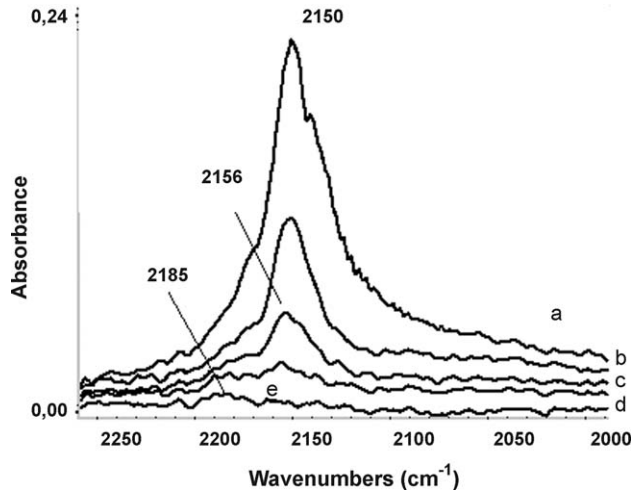

Fig. 7. IR spectra of CO adsorbed at low temperature on calcined ZnAl hydrotalcite (upper spectrum, in contact with CO gas at 130 K, lower spectra upon warming up to 200 K).

The interaction of methanol over the calcined mixed oxide gives rise to two kinds of surface methoxy groups, characterized by C–O stretching modes at ~1094 and ~1035 cm^{-1}, respectively, which is located near an additional component ~1190 cm^{-1}, which is due to a methyl rocking mode. As for comparison, we can note that the C–O stretching of methoxy groups on γ-Al_2O_3 is found at 1095 cm^{-1} [38], and those on ZnO and ZnO-based systems [39,40] range between 1080 and 1050 cm^{-1}. However, pertinent information is also obtained by the analysis of the CH stretching mode. In this region two main sharp bands originate from the splitting of the symmetric CH_3 stretching by Fermi resonance with the first overtone of the corresponding symmetric deformation [41,42].

From spectrum in Fig. 9d is evident that the CO stretching mode at 1034 cm^{-1} corresponds to the couple of $\nu_{sym}CH_3$ modes at 2950 and 2845 cm^{-1}, both weak (Species A). On the contrary, the CO stretching mode at ~1090 cm^{-1} corresponds the couple of $\nu_{sym}CH_3$ modes at ~2940 and ~2820 cm^{-1}, relatively stronger (species B).

These results do not fully match, apparently with those arising from methoxy groups (thought to be bridging) on γ-Al_2O_3 where the CO stretching mode 1095 cm^{-1} correspond to $\nu_{sym}CH_3$ modes at 2955, 2844 cm^{-1}, while on ZnO the CO stretching mode 1076 cm^{-1} correspond to $\nu_{sym}CH_3$ modes at 2932, 2818 cm^{-1}. It seems that the positions of CO and CH_3 modes are reversed on pure oxides with respect to the present case. According to previous studies, the lower frequency for the CH_3 modes points to a marked interaction of the C–H bonding orbitals with the oxygen lone pairs and eventually suggests a monodentate structure for such groups [38], and also the lower electronegativity of the cations bonded to methoxy group [43]. On the other hand, authors agree suggesting

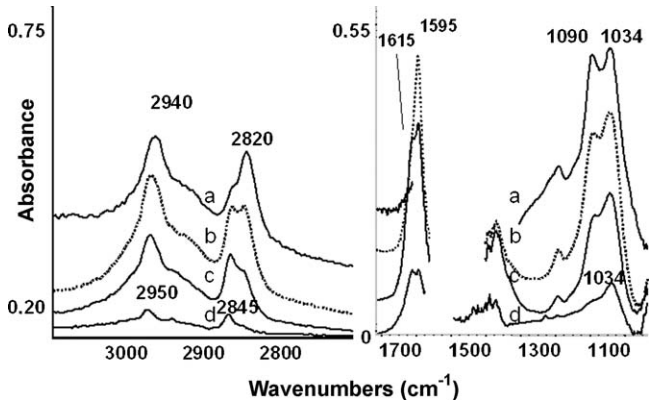

Fig. 9. IR spectra of the adsorbed species arising from contact of calcined ZnAl hydrotalcite with methanol 10 Torr at r.t. (a), 250 °C (b), 300 °C (c) and 350 °C (d).

that CO stretching mode on a single metal oxide follow the sequence terminal > bridging > triply bridging [44]. These data suggest us to assign the bands at 2940, 2820 and 1090 cm^{-1} (species B) to terminal methoxy groups, and the bands at 2950, 2845 and 1034 cm^{-1} (species A) to bridging or triply bridging methoxy groups.

The spectroscopic information can be crossed with the information on the chemical behavior of the two species. The data shown in Figs. 8 and 9 may show an higher lability of species B to decomposition to CO and hydrogen (a typical reactivity of ZnO-based catalysts [39,40]), and the higher lability of species A to desorption, likely associated to the evolution of dimethylether, a typical reactivity of alumina.

Thus we assign species A to bridging species involving either Al ions or Zn and Al ions, and species B to terminal methoxy groups on Zn ions.

Taking into account that the position of the C–O stretching mode, that depends largely from the C–O bond order, and on the electron density on this bond, we can suggest that a family of very basic and nucleophilic methoxy groups, i.e. species B, are formed over this catalyst. In particular these species appear to be more ionic than those observed previously on Al_2O_3, ZnO and stoichiometric $ZnAl_2O_4$.

4. Conclusions

This paper describes the synthesis of monophasic ZnAl HT, with composition: $[Zn_{0.67}Al_{0.33}(OH)_2](CO_3)_{0.165}{\cdot}0.5H_2O$. XRPD with Rietveld analysis are interpreted on the basis of a random distribution of Zn al Al in the 3a Wyckoff sites and a slight cell expansion with respect to Mg–Al HT.

Calcination of this material at 450 °C gives rise to a mixed oxide whose XRPD may be interpreted as being due to microcrystalline/poorly crystallized ZnO. Skeletal IR spectra, however, show the presence of spinel-like domains.

This material appears to be covered by ZnO-like surface, where Zn is predominantly in an unsaturated octahedral coordination (like is in the hydrotalcite-like precursor). The Lewis acid sites on this surface are very weak. On the contrary, the stability of carbonates to desorb shows that basicity is very high. This suggests that this material may behave as an acid–base catalyst where basicity predominates over acidity.

Methanol adsorption gives rise to the formation of terminal alcoholate species characterized by strong ionicity, together with a bridging species. This may be significant with respect to the high catalytic activity of this material to transesterification of triglycerides with methanol and polyethoxylation of fatty alcohols with ethylene oxide.

Further thermal treatments produce a mixture of well crystallized ZnO and $ZnAl_2O_4$.

Acknowledgement

This work has been supported by MIUR – PRIN.

References

[1] K. Tanabe, K. Shimazu, H. Hattori, K.i. Shimazu, J. Catal. 57 (1979) 35.
[2] P.F. Rossi, G. Busca, V. Lorenzelli, M. Waquif, O. Saur, J.C. Lavalley, Langmuir 7 (1991) 2677.
[3] K. Tanabe, W.F. Hölderich, Appl. Catal. A: Gen. 181 (1999) 399–434.
[4] G. Busca, Ind. Eng. Chem. Res. 48 (2009) 6486.
[5] L. Bournay, D. Casanave, B. Delfort, G. Hillion, J.A. Chodorge, Catal. Today 106 (2005) 190.
[6] W. Breuer, H.C. Raths, US patent 5326891 (1994) to Henkel.
[7] G. Wolf, B. Burkhart, G. Lauth, H. Trapp, A. Oftring, US patent 5741947 (1998) to BASF.
[8] B.M. Welch, US Patent 4620053 (1986) to Phillips Petroleum Company.
[9] M.V. Twigg, Catalyst Handbook, 2nd ed., Wolfe Pub, London, 1989.
[10] http://www.topsoe.com.
[11] M. Turco, G. Bagnasco, U. Costantino, F. Marmottini, T. Montanari, G. Ramis, G. Busca, J. Catal. 228 (2004) 43.
[12] Gulf Pub. Co., Hydrocarbon Processing: Gas Processes, 2004.
[13] C. Resini, T. Montanari, L. Barattini, G. Ramis, G. Busca, S. Presto, P. Riani, R. Marazza, M. Sisani, F. Marmottini, U. Costantino, Appl. Catal. A: Gen. 355 (2009) 83.
[14] A. Vaccari, Appl. Clay Sci. 14 (1999) 161.
[15] D. Tichit, B. Coq, CATTECH 7 (2003) 206.
[16] A. Corma, S. Iborra, Adv. Catal. 49 (2006) 239.
[17] D.P. Debecker, E.M. Gaigneaux, G. Busca, Chem. Eur. J. 15 (2009) 3920.
[18] U. Costantino, M. Nocchetti, F. Marmottini, R. Vivani, Eur. J. Inorg. Chem. (1999) 1439.
[19] C. Larson, R.B. von Dreele, Generalized Crystal Structure Analysis System, Los Alamos National Laboratory, NM, 2001.
[20] P. Thompson, D.E. Cox, J.B. Hastings, J. Appl. Crystallogr. 20 (1987) 79.
[21] R.L. Frost, W.N. Martens, K.L. Erickson, J. Therm. Anal. Calorim. 82 (2005) 603.
[22] P. Benito, I. Guinea, F.M. Labajos, J. Rocha, V. Rives, Micropor. Mesopor. Mater. 110 (2008) 292.
[23] P. Benito, M. Herrero, C. Barriga, F.M. Labajos, V. Rives, Inorg. Chem. 47 (2008) 5453.
[24] P.J. Sideris, U.G. Nielsen, Z. Gan, C.P. Grey, Science 321 (2008) 113.
[25] J.T. Kloprogge, L. Hockey, R.L. Frost, J. Solid State Chem. 177 (2004) 4047.
[26] F. Pascale, S. Tosoni, C. Zicovich-Wiklson, P. Ugliengo, R. Orlando, R. Dovesi, Chem. Phys. Lett. 396 (2004) 308.
[27] M.I. Baneeva, S.V. Popova, Geokhimiya (1969) 1014.
[28] G.M. Lombardo, G. Pappalardo, F. Costantino, U. Costantino, M. Sisani, Chem. Mater. 20 (2008) 5585.
[29] M. Andrés Vergés, A. Mifsud, C.J. Serna, J. Chem. Soc., Faraday Trans. 86 (1990) 959.
[30] G. Busca, in: S.D. Jackson, J.S.J. Hargreaves (Eds.), Metal Oxide Catalysis, vol. 1, Wiley–VCH, 2009,, p. 95.
[31] J. Preudhomme, P. Tarte, Spectrochim. Acta 27A (1971) 1817.
[32] H.D. Lutz, M. Feher, Spectrochim. Acta 27A (1971) 357.
[33] A. Chopelas, A.M. Hofmeister, Phys. Chem. Miner. 18 (1991) 279.
[34] C.M. Fang, C.K. Loong, G.A. de Wijs, G. de With, Phys. Rev. B 66 (2002) 144301.
[35] G. Busca, V. Lorenzelli, V. Sanchez Escribano, R. Guidetti, J. Catal. 131 (1991) 167.
[36] G. Busca, V. Lorenzelli, G. Ramis, R.J. Willey, Langmuir 9 (1993) 1492.
[37] H. Knözinger, P. Ratnasamy, Catal. Rev. Sci. Eng. 17 (1978) 31.
[38] G. Busca, P.F. Rossi, V. Lorenzelli, M. Benaissa, J. Travert, J.C. Lavalley, J. Phys. Chem. 89 (1985) 5433.
[39] A. Riva, F. Trifirò, A. Vaccari, L. Mintchev, G. Busca, J. Chem. Soc., Faraday Trans. 1 84 (1988) 1423.
[40] C. Chauvin, J. Saussey, J.-C. Lavalley, H. Idriss, J.P. Hindermann, A. Kiennemann, P. Chaumette, P. Courty, J. Catal. 121 (1990) 56.
[41] J. Derouault, J. Le Calve, M.T. Forel, Spectrochim. Acta 28A (1972) 359.
[42] J.C. Lavalley, N. Sheppard, Spectrochim. Acta 28A (1973) 2091.
[43] N. Takezawa, H. Kobayashi, J. Catal. 25 (1972) 179.
[44] M. Daturi, E. Finocchio, C. Binet, J.C. Lavalley, F. Fally, V. Perrichon, H. Vidal, N. Hockey, J. Kaspar, J. Phys. Chem. 104 (2000) 9186.